HHS Public Access

Author manuscript

Anal Chem. Author manuscript; available in PMC 2020 December 03.

Published in final edited form as:

Anal Chem. 2019 December 03; 91(23): 15240–15247. doi:10.1021/acs.analchem.9b04217.

Photopatterned Membranes and Chemical Gradients Enable Scalable Phenotypic Organization of Primary Human Colon Epithelial Models

Samuel S. Hinman[†], **Yuli Wang**[†], **Nancy L. Allbritton**[†,‡,§,*]

[†]Department of Chemistry, University of North Carolina at Chapel Hill, Chapel Hill, NC 27599, USA

[‡]Joint Department of Biomedical Engineering, University of North Carolina at Chapel Hill, Chapel Hill, NC 27599, and North Carolina State University, Raleigh, NC 27607, USA

Abstract

Biochemical gradients across the intestinal epithelium play a major role in governing intestinal stem cell compartmentalization, differentiation dynamics, and organ-level self-renewal. However, scalable platforms that recapitulate the architecture and gradients present *in vivo* are absent. We present a platform in which individually addressable arrays of chemical gradients along the intestinal crypt long axis can be generated, enabling scalable culture of primary *in vitro* colonic epithelial replicas. The platform utilizes standardized well plate spacing, maintains access to basal and luminal compartments, and relies on a photopatterned porous membrane to act as diffusion windows while supporting the *in vitro* crypts. Simultaneous fabrication of 3,875 crypts over a single membrane was developed. Growth factor gradients were modelled and then experimentally optimized to promote long-term health and self-renewal of the crypts which were assayed *in situ* by confocal fluorescence microscopy. The cultured *in vitro* crypt arrays successfully recapitulated the architecture and luminal-to-basal phenotypic polarity observed *in vivo*. Furthermore, known signaling regulators (*e.g.*, butyrate and DAPT) produced measurable and predictable effects on the organized cell compartments, each decreasing crypt proliferation in the basal regions to negligible values. This platform is readily adaptable to the screening of tissue from individual patients to assay the impact of food and bacterial metabolites and/or drugs on colonic crypt dynamics. Importantly, the cassette is compatible with a wide range of sensing/detection modalities, and the developed fabrication methods should find applications for other cell and tissue types.

Graphical Abstract

[*]**Corresponding Author**: nlallbri@unc.edu.

[§]Department of Bioengineering, University of Washington, Seattle, WA 98195, USA

Supporting Information

The Supporting Information is available free of charge on the ACS Publications website at DOI:10.1021/acs.analchem.9b04217. Experimental details, including buffer and media compositions, poly(dimethylsiloxane) stamp fabrication for collagen micromolding, modeling of chemical gradients, maintenance of primary colonic epithelial cells, and fluorescence staining. Supplemental discussion, covering impact of chemical gradients of planar monolayers of cells, and considerations for *in vitro* crypt screening by confocal microscopy. Additional data, including characterizations of the collagen scaffold and assembled device, diffusion measurements, imaging parameters, and impact of Notch gradients on planar monolayers of cells.

N.L.A. and Y.W. have a financial interest in Altis Biosystems, Inc. S.S.H. declares no competing financial interests.

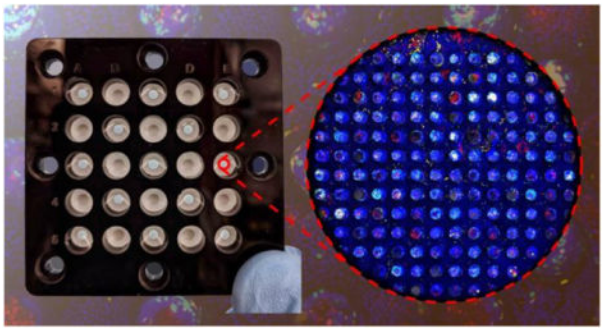

INTRODUCTION

Gradients shape human physiology through intricate balances of biomolecular messengers and physicomechanical cues. Within the large intestine (*i.e.*, colon), a multitude of growth factor, metabolite, gas, and extracellular matrix gradients exist across the epithelium that govern the composition and organization of various cell types, thus influencing organ-level self-renewal and function.[1–2] The colonic epithelium is organized into a series of crypts, invaginations present throughout the length of the organ with stem cells located at each crypt base.[3–4] The stem cells give rise to a population of proliferative transit amplifying cells before terminally differentiating into absorptive or secretory (*e.g.*, goblet and enteroendocrine) lineages at the luminal surface.[5–6] Studies connecting diet, gut microbiota, and crypt homeostasis have far-reaching implications in our understanding of the pathophysiology of inflammatory bowel diseases and colorectal cancer.[7] As such, the development of scalable and physiologically relevant intestinal models that enable increased throughput and high content information regarding crypt cellular behaviors is of high importance to the food and pharma sectors.[8]

In vitro intestinal models are currently limited in their compatibility with analytical methods (*e.g.*, standardized plate assays, high-throughput automation), ease of sampling, and/or applicability to human disease.[9] Immortalized cell lines remain gold standard models of the intestinal epithelium in the pharmaceutical industry,[10–11] yet fail to recapitulate key aspects of the *in vivo* tissue.[12] The isolation, expansion, and culture of primary intestinal stem cells has been made possible through a combination of media supplementation with selected biochemical growth factors (*e.g.*, EGF, Wnt3a, R-spondin, and noggin) when combined with growth within a hydrogel.[13–14] Under these conditions, harvested individual intestinal stem cells form spherical organoids possessing the complete suite of stem/proliferative and differentiated cell types found in the *in vivo* colon.[15] These human cells maintain the genotype as well as many physiologic properties of the original host.[16] However, the organoids lack fully organized crypt microenvironments, as well as accessible luminal regions.

Among a variety of primary cell-derived organ replica systems,[17–19] *in vitro* intestinal crypt arrays have emerged as a promising technology for understanding intestinal homeostasis and drivers of stem cell fate decisions.[20–24] With this platform, primary intestinal cells from clinical biopsies can be cultured on a shaped hydrogel scaffold formed to mimic the crypt

architecture and density observed *in vivo*. Crucial to proper crypt polarization are chemical gradients of growth or differentiation factors spanning the crypt long axis, driving localization of the stem/proliferative cells to the crypt base and differentiated cell types to the luminal crypt region. A significant advantage of the *in vitro* crypt platform is that basal and luminal compartments remain accessible for reagent addition, sampling, and/or subsequent assays. Prior versions of the *in vitro* crypts were constructed on a small scale due to the demanding fabrication methods and challenging optical conditions. Here, we have developed scalable scaffold fabrication strategies, parallelizable *in vitro* crypt formation methods, as well as enhanced *in situ* analytical protocols for the *in vitro* crypts. Beyond permitting multiple *z*-axial biochemical gradients to be imposed simultaneously across crypts in distinct regions, the device was compatible with confocal microscopy so that crypt cell behavior was readily assayed, maximizing throughput of the three-dimensional intestinal replicas.

EXPERIMENTAL SECTION

Culture Device Fabrication.

The culture device was designed using Autodesk Fusion 360 (San Rafael, CA) and Adobe Illustrator CC 2018 (San Jose, CA). The device consisted of four components held together with stainless steel screws and sealed with a biocompatible transfer adhesive (1504XL, 3M): an opaque acrylic cassette for cell and luminal media containment (8505K754, McMaster-Carr), a patterned membrane, a silicone gasket defining the basal media reservoirs (86045K77, McMaster-Carr), and a transparent acrylic base plate (8560K239, McMaster-Carr). Acrylic and silicone components were laser cut (ILS9.75, Universal Laser Systems) and incubated in 1% (w/v) Alconox overnight to remove manufacturing contaminants.

Hydrophilic PTFE membranes (BGCM00010, Millipore-Sigma) were patterned with EPON™ 1002F (Miller-Stephenson) by photolithography. The membranes were mounted to glass slides (260234, Ted Pella, Inc.) using polyimide tape. 1002F formulation 50 (1002F-50) photoresist was prepared,[25] incubated throughout the membrane for 2 min, and spin coated (Model WS-650MZ-23NPP, Laurell Technologies Corp.) at 2000 rpm for 30 s to remove excess photoresist and generate an even film. Solvent was removed by baking for 50 min at 95 °C. The photoresist-impregnated membranes were exposed to ultraviolet light (350 mJ) through a photomask (Front Range Photomask, Lake Havasu City, AZ) possessing an array of opaque circles (dia.: 3 mm; pitch: 9 mm) to define the growth factor diffusion windows. The membranes were subjected to sequential 5 min bake steps at 95 °C and 120 °C, prior to development in propylene glycol methyl ether acetate (PGMEA) for 6 min. Patterned membranes were thereafter incubated for ≥16 h in deionized (DI) water to delaminate the membranes from the glass support.[26] The final thickness of the material was 85 μm, with the cured photoresist extending 45 μm above the PTFE surface (LEXT OLS5000, Olympus Corp.)

Patterned membranes were manually fixed to cassettes with transfer adhesive (thickness: 0.11 mm) at ambient temperature and pressure to form the luminal reservoirs, and shaped scaffolds of crosslinked collagen were micromolded within each luminal well for *in vitro* crypt culture (Supporting Information).[22] All components were cleansed in 75% (v/v)

ethanol for 5 min and transferred into an aseptic tissue culture hood for final device assembly. Micromolded collagen scaffolds were coated with 10 μg mL^{-1} rat tail collagen (354236, Corning) in 1× PBS overnight at 37 °C,[22] and rinsed once with 1× PBS prior to cell plating.

Culture of Primary Human Colon Epithelial Cells.

The human colonic epithelial biopsy specimen (male, 52 y) was obtained during a routine screening colonoscopy performed at the University of North Carolina (UNC) Hospitals Meadowmount Endoscopy Center under UNC IRB #14–2013. The epithelial were cells expanded following a previously reported monolayer culture protocol (Supporting Information).[27] For each culture device, cells were passaged from two (19.2 cm^2) wells (≥80% confluency) of a 6-well maintenance/expansion plate. *In vitro* crypt cultures were expanded for 8 d (EM_{basal}/$EM_{luminal}$, Table S1, Supporting Information) and thereafter subjected to growth factor gradients for 4 d (SM_{basal}/$DM_{luminal}$, Table S1, Supporting Information), with media changes occurring every 24 h after passaging. For investigations involving Notch signaling regulation, sodium butyrate (5 mM, 303410, Millipore-Sigma) or DAPT (10 μM, M60023–5, Xcess Biosciences) was added to luminal DM.[28–29]

Image Acquisition and Analysis.

Once cell cultures were fixed and fluorescently labelled (Supporting Information), confocal fluorescence microscopy was performed on an inverted Olympus Fluoview 3000 (Waltham, WA) equipped with 405 nm, 488 nm, 561 nm, and 640 nm laser diodes, in conjunction with a 4× (N.A. 0.16, UPLSAPO) or 20× (N.A. 0.45, LUCPLFLN) objective and a galvanometer scanner. Emission wavelengths (Hoechst: 430–470 nm, Cy5: 650–750 nm, AF 488: 505–545 nm, Texas Red: 600–640 nm) were selected from manufacturer provided control software. *Z*-stacks were performed over manually defined regions spanning the entire *in vitro* crypt depth with software-optimized step sizes.

Image stacks were subjected to three-dimensional constrained iterative deconvolution in cellSens Dimension v1.18 (Olympus Corp.) utilizing 20 iterations of an advanced maximum likelihood algorithm (Figure S2, Supporting Information). Images were imported into Fiji,[30] in which each fluorescence channel was converted to binary through empirical thresholding and individual crypts were assigned to circular 75 pixel diameter regions of interest (Figure S10, Supporting Information). Crypts that did not occupy the full depth of the scaffold were omitted from analysis, accounting for 44 ± 19 crypts per well (mean ± S.D., *ca.* 29% of total crypts). The average area occupied by the suprathreshold level of fluorescence was measured for each ROI and slice throughout the stack, and measurements were exported to Origin 9.0 (OriginLab Corp., Northampton, MA). Extracted suprathreshold area values for EdU, Muc2, and ALP were normalized to that of Hoechst 33342. All *in vitro* crypt heights were normalized between 0 (base) and 1 (lumen). Within each well/set of gradients, fluorescence distributions along the *z*-axis for *in vitro* crypts were averaged and plotted as stacked distribution plots, with area under curve analyses performed for selected compartments along the *z*-axis. All reported data are from $n = 3$ devices.

Statistical Analysis.

All statistical analyses were performed using GraphPad Prism 8.1.2 (GraphPad Software, San Diego, CA) at a significance level (α) of 0.05. For edge effect tests, one-way ANOVA was used followed by Tukey's test for multiple comparisons. For comparing the combined effects of L-WRN gradients and Notch signaling regulators, two-way ANOVA was used followed by Tukey's test for multiple comparisons. Unless specified, data are presented as sample means with error bars depicting standard error of the mean, and for statistical comparisons, p values are represented as follows: * for $p \leq 0.05$, ** for $p < 0.01$, and *** for $p < 0.001$. G*Power v3.1.9.2 (Heinrich Heine University, Germany) was used for *a priori* sample size estimation based off of a two-tailed t-test for differences in EdU^+ cells between adjacent *z*-regions from prior data, with $\alpha = 0.05$ and power $(1-\beta) = 0.95$.[22, 31]

RESULTS AND DISCUSSION

Design Specifications for Scalable Culture of *In Vitro* Crypts.

Generation of individually addressable *z*-axial linear gradients is required to maintain crypts polarized into stem/proliferative and differentiated zones. The formation of these gradients at minimum requires a cassette housing both basal and luminal compartments, forming a stable source and sink for nutrients over an extended time frame (benchmark: 24 h). An integrated porous membrane performs dual roles: separating the source and sink reservoirs to establish the growth factor and metabolite gradients, and acting as a physical support for shaped scaffolds that mimic the architecture of *in vivo* crypts. To enhance adoption by others, incorporation of standardized 96-well spacing and geometry is desirable to increase throughput while enabling ease of integration with pre-existing assays and instrumentation. While it is noted that several commercial options based on Boyden chambers exist, the basket insert design results in decreased luminal compartment volume preventing the luminal reservoir from being acting as an effective sink during crypt polarization. Furthermore, the limited luminal access area in these commercial assemblies is not compatible with the molding process used to shape crypt scaffolds. For these reasons, a luminal cassette underlaid by a patterned polytetrafluoroethylene (PTFE) membrane was designed to maximize apical accessibility and well volumes. The luminal cassette is secured over a series of shared basal reservoirs defined by a laser cut silicone gasket (Figure 1A), which can be cut to any desired shape for fine control of basal compartment dimensions, tailored to the experiment being performed.[32] Finally, a transparent base plate is held in conformal contact beneath the gasket, allowing for *in situ* monitoring of cells by bright field microscopy in order to assess their health throughout culture. Where specified (Figure 1A), components are sealed together with a biocompatible transfer adhesive to prevent leakage (Figure S3, Supporting Information).[33–34]

Photolithographic Patterning of PTFE.

Membranes of hydrophilic PTFE were selected for gradient formation due to their optical transparency and high permeability. Photolithography has previously been demonstrated to be suitable for photopatterning SU-8 into chromatography paper.[35] 1002F resin, a close relative of SU-8, possesses high optical transparency with the ability be patterned into biocompatible structures.[25] Furthermore, 1002F exhibits lower background fluorescence and

is less brittle than other polymers, increasing the practicality of the device for *in situ* imaging of cultures. The PTFE membranes were incubated in a 1002F photoresist to impregnate the resin throughout (Figure 1B), and thereafter patterned using standard photolithographic processing. Once complete, membrane areas that were impregnated with cured photoresist were water-impermeable, while non-patterned areas remained water-permeable (Figure S3–S4, Supporting Information). These methods for patterning hydrophilic PTFE were robust and reproducible for obtaining the features desired herein (20/20 of membranes exhibited pattern transfer, Figure 1C), and were successfully extended to other fibrous substrates with no modification (Figure S4, Supporting Information).

Fabrication of a Multiplexed Gradient Cassette Possessing Crypt Scaffolds.

Prior iterations of the *in vitro* crypt platform relied on serially micromolding Type 1 collagen scaffolds to generate the architectural features of the intestinal epithelium.[20–22] In scaling scaffold fabrication, serial molding and cross-linking did not yield reproducible crypt arrays (*ca.* 15% failure rate). Therefore, the process was modified to utilize a polydimethylsiloxane (PDMS) stamp generated through soft lithography that could generate all crypt structures within each well of the device in parallel (Figure 2A, Supporting Information for fabrication). In addition to lowering the failure rate of micromolding to *ca.* 5% of crypt array elements or microwells, reproducibility of these features within collagen was excellent, with average crypt heights exhibiting 1.59 % relative standard deviation (RSD, 419.1 ± 6.6 μm, n = 128), basal diameters exhibiting 9.63 % RSD (65.4 ± 6.3 μm, n = 125), and luminal diameters exhibiting 4.62 % RSD (128.1 ± 5.9 μm, n = 125). Up to 25 scaffolds housed within separate wells could be generated at once in this manner (Figure 2B and S5, Supporting Information), only limited by the gelation time of collagen in the presence of crosslinking reagents (*ca.* 5 min).

Diffusion profiles for 40 kDa fluorescein-dextran were modeled for the device to determine optimum parameters under which the membrane would form a semi-infinite boundary between reservoirs to polarize crypts (Figure 2C, 2D, also Supporting Information).[36] The specific size of dextran was selected for its close proximity to Wnt3a (39.7 kDa), R-spondin (40.0 kDa) and Noggin (46 kDa), the major growth factors responsible for maintaining the stem cell niche *in vivo*.[13, 37] These experiments demonstrated that by restricting the diffusion window between each basal and luminal compartment from 32 mm^2 to 7.07 mm^2, a steep gradient of these growth factors can be generated that varied by ≤10 % over 24 h (Figure 2E, 2F). Once the physical device was completely assembled, the diffusion profiles of fluorescein-dextran (40 kDa) matched with those that were predicted by the COMSOL simulations (Figure 2E), demonstrating that this device can be used to generate scalable arrays of z-axial gradients with an exchange of the luminal and basal media every 24 h.

Characterization of Lateral Edge Effects.

To assess whether edge error mitigation schemes would be necessary,[38] all wells were subjected to identical gradients of a fluorescent dextran (40 kDa, 100 μg mL^{-1} basal, 0 μg mL^{-1} luminal) and luminal fluorescence intensities were compared after incubating for 24 h at 37 °C. Fluorescence intensities were averaged between wells from different areas and patterns across the device (Figure 3A), and no significant differences were noted ($p > 0.2$,

one-way ANOVA) (Figure 3B). To further confirm that conclusions drawn from living cells cultured in the device would not be impacted by well location, planar monolayers of primary, human colonic epithelial cells were formed directly over permeable areas of the patterned membranes and investigated for variations in their proliferative capacities and differentiation when exposed to identical growth factor gradients. Cells were seeded and expanded over the ECM-coated membranes within the device,[2, 39] and growth factor gradients were imposed for 4 d, during which, a differentiation medium (DM, $WRN^{-/-/-}$, Supporting Information) was added to the luminal compartments, and a stem cell supporting growth medium (SM, $WRN^{+/+/+}$, Supporting Information) was added to the basal reservoirs, which were exchanged every 24 h (Supporting Information). Relative amounts of stem/proliferative (EdU^+, Figure 3C,E) and differentiated ($KRT20^+$, Figure 3D,E) cells were quantified and no significant differences for stem/proliferative ($p > 0.99$, one-way ANOVA) or differentiated ($p > 0.48$, one-way ANOVA) markers were noted between wells from different areas and patterns across the array, suggesting that the same conditions can be generated independent of their well location (Figure S6, Supporting Information for additional patterns).

Generation of *In Vitro* Colonic Crypt Arrays.

The presence of a stem/proliferative compartment at the base of each intestinal crypt is known to drive self-renewal of the tissue *in vivo*, with non-dividing, terminally differentiated cells carrying out absorptive and secretory functions at the luminal surface.[2] The scaffolds were micromolded in a 5×3 pattern (Figure 2B), leaving the top and bottom rows open for basal compartment access, and colonic stem/proliferative cells were seeded onto each luminal array element. Intestinal epithelial stem cells were isolated from primary tissue and expanded on the shaped scaffolds for 8 d under EM ($WRN^{+/+/+}$, Supporting Information) until the cells grew into the crypt microwells and covered the entirety of the array surface (Figure 4B). A gradient of growth factors was then formed across the *in vitro* crypts ($SM_{basal}/DM_{luminal}$, Supporting Information) for 4 d with a medium exchange every 24 h (Figure 4A,B). Proliferative cells (EdU^+) were restricted to the basal region of the crypts while differentiated colonocytes (ALP^+) were present at the luminal plane (Figure 4C). Alkaline phosphatase is expressed on the epithelial cell surface,[40] as well as a secreted red precipitate formed by the action of ALP during the labeling process, which was observed within the hollow lumen of the *in vitro* crypts (Figure 4C and S8, Supporting Information). Mucin-2 ($Muc2^+$), secreted by goblet cells found throughput the intestine, was also present. Further evidence for *in vitro* generation of distinct stem/proliferative and differentiated cell regions is presented through localized expression of Olfm4, a marker expressed by colonic epithelial stem cells at the crypt base, and KRT20, which is upregulated within differentiated cells at the luminal plane (Figure 4C). Multiple proteins responsible for tight junction maintenance between adjacent cells, ZO-1 and E-cadherin, were prominently displayed at the luminal plane, suggesting that this system could be used to study barrier integrity and function (Figure 4C).

Impact of Chemical Gradients on *Z*-Axial Phenotypic Distributions within *In Vitro* Crypts.

The microbial metabolite, butyrate, provides a dual role within the colonic epithelium, acting as a primary energy source for absorptive colonocytes while inhibiting stem/

proliferative activity at physiologic concentrations.[41] As the design of this system allows for direct *in vitro* investigations to be performed on the interplay between the biochemical gradients and anatomical microstructures observed *in vivo*, we sought to characterize these interactions further by varying the levels of growth factors supporting the stem cell niche (0 – 50% L-WRN conditioned medium[42]) against a physiologic concentration (5 mM) of butyrate. DAPT, playing an opposite role to butyrate in Notch signaling,[28–29] was also included in the study to test whether similar differential effects on stem/proliferative and differentiated cell populations would be observed.

The *in vitro* crypt cultures were imaged in manner optimized for three-dimensional screening (Table S2, Figure S2, Supporting Information). The amount of EdU^+ cells was greatest for culture sites possessing the steepest WRN gradients due to WRN at high concentration in the basal reservoir. In these cultures, EdU^+ cells were at the greatest density at the crypt base and declining in number towards the luminal crypt region, consistent with prior reports of the impact of WRN gradients on cell compartmentalization within crypts (Figure 5A).[22] Both butyrate-containing (DM-B) and DAPT-containing (DM-D) luminal differentiation media severely diminished this stem/proliferative activity (Figure 5A). In order to more thoroughly evaluate region-specific effects on proliferation, the crypts were divided into thirds (*e.g.*, basal, middle, and luminal) for which area under curve (AUC) analyses of normalized fluorescence were plotted (Figure 5B). The basal third harbors the majority of proliferative activity, with *ca.* 1 order of magnitude more EdU^+ cells than the middle region and *ca.* 2 orders of magnitude more than the luminal region (Figure 5B). Butyrate (DM-B) inhibited proliferation with the greatest potency in the lowest region. This inhibition was most significant for all regions under conditions in which higher amounts (25 – 50%) of basal L-WRN were present (Figure 5B).

Intriguingly, while DAPT (DM-D) exhibited a similar pattern of proliferative inhibition as butyrate (DM-B) for the basal third of the crypts, expression of EdU^+ cells was increased for DAPT-exposed cells relative to that for butyrate in the middle and luminal regions (Figure 5B), though ALP and Muc2 presence are not significantly affected ($p > 0.2$, Figure 5D and S9, Supporting Information). It is possible that DAPT targets a specific subtype(s) of proliferative cell within the lowest region (*e.g.*, $Lgr5^+$ crypt base columnar cells or +4 label-retaining cells) with greater efficacy than it does proliferative transit amplifying cells (*e.g.*, absorptive progenitor or $DLL1^+$ secretory progenitor) in the middle and luminal regions.[43–45] While other reports have suggested that certain Notch regulators, including DAPT, target $Lgr5^+$ crypt base columnar cells over other cell types,[46] further studies may be warranted utilizing the methods developed herein.

In contrast to proliferative (EdU^+) activity, absorptive colonocyte (ALP^+) activity was limited at the luminal plane unless differentiation was induced by the presence of butyrate (Figure 5C,D). Luminal ALP induction by butyrate was consistent among all conditions in which a basal supply of WRN was present (12.5 – 50% basal L-WRN), though does not occur in $WRN^{-/-/-}$ conditions (0% basal L-WRN). While there appears to be constant ALP^+ fluorescence within the basal region of the crypts (lower 50%), no significant patterns are noted for this region under any treatment. This data is in agreement with the excised *in vitro* crypt measurements (Figure 4C), and provides further evidence that this may be due to the

presence of secreted reaction precipitate within the crypt lumen (Figure S8, Supporting Information). The ability to simultaneously survey the impact of a multitude of gradients enabled rapid assessment of the impact of butyrate on crypt polarization and cell compartmentalization within the distinct crypt zones. Further, the impact of butyrate on intestinal stem cell differentiation within colonic crypts suggested that the presence of a stem/proliferative niche may be necessary for maintenance of a full suite of cell types within this platform.

CONCLUSIONS

Few options exist for modeling the intestinal epithelium with primary cells derived from human subjects, and culture formats that support both the microscale architecture and biochemical environment encountered *in vivo* are challenging. In this work, lateral arrays of *z*-axial growth factor and metabolite gradients were applied across *in vitro* colonic crypt epithelia in parallel, revealing the interplay between these opposing gradients and how they impact the distribution of cellular phenotypes. The throughput of these experiments and analyses were enabled by the development of a photopatterned membrane, which acted to segregate basal and luminal compartments, and was designed to maintain sharp gradient profiles throughout culture. In addition to being able to support growth of planar monolayer intestinal cell cultures, the device supported formation of *in vitro* crypts that exhibited many of the hallmark biomarker distributions observed *in vivo*.[6] The presence of distinct stem/proliferative niche and differentiated regions were readily identified, which were differentially regulated by opposing gradients of stem cell supporting growth factors (*i.e.*, WRN) and Notch signaling regulators. Similar effects have been reported for opposing levels of Wnt3a and bone morphogenetic protein 4 (BMP4) over primary intestinal cells,[47] with conclusions drawn that these two molecules form an intrinsic feedback circuit regulating self-renewal: the platform developed herein could be exploited for further investigations of feedback mechanisms induced by opposing gradients along the crypt axis, with new biological discoveries strengthened by the inclusion of additional primary cell donors of different genders, ages, and disease states.[16] Beyond chemical gradients, stem cell fate decisions have been partially ascribed to the mechanical properties (*e.g.*, stiffness, porosity) of the extracellular matrix,[14] presenting opportunities for further studies of mechanotransduction, potentially with parallel gradients of stiffness. Given that a standardized geometry (96-well) is already built into the design of this device, with further scaling and adoption of rapid, 3D microscopy techniques (*e.g.*, spinning disc confocal, light sheet), a high content platform can be envisioned that is both user-friendly and human patient-relevant.

Supplementary Material

Refer to Web version on PubMed Central for supplementary material.

ACKNOWLEDGEMENTS

The authors gratefully acknowledge financial support from the National Institute of Diabetes and Digestive and Kidney Diseases (NIDDK) of the National Institutes of Health (R01 DK109559). Laser cutting was performed within the Be A Maker (BeAM) network of makerspaces at the University of North Carolina at Chapel Hill. The

authors wish to thank Dr. Peter J. Attayek for assistance in modeling and prototyping of the culture device, and Prof. Scott T. Magness for procurement of the intestinal biopsy specimen.

REFERENCES

1. Wang Y; Kim R; Hinman SS; Zwarycz B; Magness ST; Allbritton NL, Bioengineered Systems and Designer Matrices that Recapitulate the Intestinal Stem Cell Niche. Cell. Mol. Gastroenterol. Hepatol 2018, DOI: 10.1016/j.jcmgh.2018.01.008.
2. Dutton JS; Hinman SS; Kim R; Wang Y; Allbritton NL, Primary Cell-Derived Intestinal Models: Recapitulating Physiology. Trends Biotechnol. 2018, DOI: 10.1016/j.tibtech.2018.12.001.
3. Barker N; van Es JH; Kuipers J; Kujala P; van den Born M; Cozijnsen M; Haegebarth A; Korving J; Begthel H; Peters PJ; Clevers H, Identification of stem cells in small intestine and colon by marker gene Lgr5. Nature 2007, 449 (7165), 1003–U1. [PubMed: 17934449]
4. Sangiorgi E; Capecchi MR, Bmi1 is expressed in vivo in intestinal stem cells. Nat. Genet 2008, 40 (7), 915–920. [PubMed: 18536716]
5. Hsu YC; Li LS; Fuchs E, Transit-Amplifying Cells Orchestrate Stem Cell Activity and Tissue Regeneration. Cell 2014, 157 (4), 935–949. [PubMed: 24813615]
6. Baker AM; Cereser B; Melton S; Fletcher AG; Rodriguez-Justo M; Tadrous PJ; Humphries A; Elia G; McDonald SA; Wright NA; Simons BD; Jansen M; Graham TA, Quantification of crypt and stem cell evolution in the normal and neoplastic human colon. Cell Rep. 2014, 8 (4), 940–947. [PubMed: 25127143]
7. Bultman SJ, Butyrate consumption of differentiated colonocytes in the upper crypt promotes homeostatic proliferation of stem and progenitor cells near the crypt base. Transl. Cancer Res 2016, 5 (3), S526–S528. [PubMed: 30568890]
8. Gareau MG; Sherman PM; Walker WA, Probiotics and the gut microbiota in intestinal health and disease. Nat. Rev. Gastroenterol. Hepatol 2010, 7 (9), 503–14. [PubMed: 20664519]
9. Probst C; Schneider S; Loskill P, High-throughput organ-on-a-chip systems: Current status and remaining challenges. Curr Opin Biomed Eng 2018, 6, 33–41.
10. Kaiser GC; Polk DB, Tumor necrosis factor alpha regulates proliferation in a mouse intestinal cell line. Gastroenterology 1997, 112 (4), 1231–1240. [PubMed: 9098007]
11. Artursson P; Palm K; Luthman K, Caco-2 monolayers in experimental and theoretical predictions of drug transport. Adv. Drug Del. Rev 2001, 46 (1–3), 27–43.
12. Hernandez-Gordillo V; Koppes AN; Griffith LG; Breault DT; Carrier RL, Engineering the Niche for Intestinal Regeneration In Biology and Engineering of Stem Cell Niches, Vishwakarma A; Karp J, Eds. Academic Press: London, United Kingdom, 2017, DOI: 10.1016/B978-0-12-802734-9.00037-8pp 601–615.
13. Jung P; Sato T; Merlos-Suarez A; Barriga FM; Iglesias M; Rossell D; Auer H; Gallardo M; Blasco MA; Sancho E; Clevers H; Batlle E, Isolation and in vitro expansion of human colonic stem cells. Nat. Med 2011, 17 (10), 1225–1227. [PubMed: 21892181]
14. Glorevski N; Sachs N; Manfrin A; Giger S; Bragina ME; Ordonez-Moran P; Clevers H; Lutolf MP, Designer matrices for intestinal stem cell and organoid culture. Nature 2016, 539 (7630), 560–564. [PubMed: 27851739]
15. Sato T; Clevers H, Growing Self-Organizing Mini-Guts from a Single Intestinal Stem Cell: Mechanism and Applications. Science 2013, 340 (6137), 1190–1194. [PubMed: 23744940]
16. van de Wetering M; Francies HE; Francis JM; Bounova G; Iorio F; Pronk A; van Houdt W; van Gorp J; Taylor-Weiner A; Kester L; McLaren-Douglas A; Blokker J; Jaksani S; Bartfeld S; Volckman R; van Sluis P; Li VSW; Seepo S; Pedamallu CS; Cibulskis K; Carter SL; McKenna A; Lawrence MS; Lichtenstein L; Stewart C; Koster J; Versteeg R; van Oudenaarden A; Saez-Rodriguez J; Vries RGJ; Getz G; Wessels L; Stratton MR; McDermott U; Meyerson M; Garnett MJ; Clevers H, Prospective Derivation of a Living Organoid Biobank of Colorectal Cancer Patients. Cell 2015, 161 (4), 933–945. [PubMed: 25957691]
17. Kasendra M; Tovaglieri A; Sontheimer-Phelps A; Jalili-Firoozinezhad S; Bein A; Chalkiadaki A; Scholl W; Zhang C; Rickner H; Richmond CA; Li H; Breault DT; Ingber DE, Development of a

primary human Small Intestine-on-a-Chip using biopsy-derived organoids. Sci. Rep 2018, 8. [PubMed: 29311689]

18. Greenhalgh K; Ramiro-Garcia J; Heinken A; Ullmann P; Bintener T; Pacheco MP; Baginska J; Shah P; Frachet A; Halder R; Fritz JV; Sauter T; Thiele I; Haan S; Letellier E; Wilmes P, Integrated In Vitro and In Silico Modeling Delineates the Molecular Effects of a Synbiotic Regimen on Colorectal-Cancer-Derived Cells. Cell Rep. 2019, 27 (5), 1621–+. [PubMed: 31042485]
19. Chen HJ; Wei ZB; Sun J; Bhattacharya A; Savage DJ; Serda R; Mackeyev Y; Curley SA; Bu PC; Wang LH; Chen SB; Cohen-Gould L; Huang E; Shen XL; Lipkin SM; Copeland NG; Jenkins NA; Shuler ML, A recellularized human colon model identifies cancer driver genes. Nat. Biotechnol 2016, 34 (8), 845–851. [PubMed: 27398792]
20. Wang YL; Gunasekara DB; Reed MI; DiSalvo M; Bultman SJ; Sims CE; Magness ST; Allbritton NL, A microengineered collagen scaffold for generating a polarized crypt-villus architecture of human small intestinal epithelium. Biomaterials 2017, 128, 44–55. [PubMed: 28288348]
21. Wang YL; Gunasekara DB; Attayek PJ; Reed MI; DiSalvo M; Nguyen DL; Dutton JS; Lebhar MS; Bultman SJ; Sims CE; Magness ST; Allbritton NL, In Vitro Generation of Mouse Colon Crypts. ACS Biomater. Sci. Eng 2017, 3 (10), 2502–2513. [PubMed: 30854421]
22. Wang Y; Kim R; Gunasekara DB; Reed MI; DiSalvo M; Nguyen DL; Bultman SJ; Sims CE; Magness ST; Allbritton NL, Formation of human colonic crypt array by application of chemical gradients across a shaped epithelial monolayer. Cell. Mol. Gastroenterol. Hepatol 2018, 5 (2), 113–130. [PubMed: 29693040]
23. Kim R; Wang Y; Hwang SJ; Attayek PJ; Smiddy NM; Reed MI; Sims CE; Allbritton NL, Formation of arrays of planar, murine, intestinal crypts possessing a stem/proliferative cell compartment and differentiated cell zone. Lab Chip 2018, 18 (15), 2202–2213. [PubMed: 29944153]
24. Kim R; Attayek PJ; Wang Y; Furtado KL; Tamayo R; Sims CE; Allbritton NL, An *in vitro* intestinal platform with a self-sustaining oxygen gradient to study the human gut/microbiome interface. Biofabrication 2019, DOI: 10.1088/1758-5090/ab446e.
25. Pai JH; Wang Y; Salazar GT; Sims CE; Bachman M; Li GP; Allbritton NL, Photoresist with low fluorescence for bioanalytical applications. Anal. Chem 2007, 79 (22), 8774–8780. [PubMed: 17949059]
26. Ornoff DM; Wang Y; Allbritton NL, Characterization of freestanding photoresist films for biological and MEMS applications. J. Micromech. Microeng 2013, 23 (2), 025009. [PubMed: 24072957]
27. Wang YL; DiSalvo M; Gunasekara DB; Dutton J; Proctor A; Lebhar MS; Williamson IA; Speer J; Howard RL; Smiddy NM; Bultman SJ; Sims CE; Magness ST; Allbritton NL, Self-renewing Monolayer of Primary Colonic or Rectal Epithelial Cells. Cell. Mol. Gastroenterol. Hepatol 2017, 4 (1), 165–182.e7. [PubMed: 29204504]
28. Cayo MA; Cayo AK; Jarjour SM; Chen H, Sodium butyrate activates Notch1 signaling, reduces tumor markers, and induces cell cycle arrest and apoptosis in pheochromocytoma. Am. J. Transl. Res 2009, 1 (2), 178–183. [PubMed: 19956429]
29. Geling A; Steiner H; Willem M; Bally-Cuif L; Haass C, A gamma-secretase inhibitor blocks Notch signaling in vivo and causes a severe neurogenic phenotype in zebrafish. EMBO Rep 2002, 3 (7), 688–94. [PubMed: 12101103]
30. Schindelin J; Arganda-Carreras I; Frise E; Kaynig V; Longair M; Pietzsch T; Preibisch S; Rueden C; Saalfeld S; Schmid B; Tinevez JY; White DJ; Hartenstein V; Eliceiri K; Tomancak P; Cardona A, Fiji: an open-source platform for biological-image analysis. Nat. Methods 2012, 9 (7), 676–682. [PubMed: 22743772]
31. Faul F; Erdfelder E; Lang AG; Buchner A, G*Power 3: a flexible statistical power analysis program for the social, behavioral, and biomedical sciences. Behav. Res. Methods 2007, 39 (2), 175–91. [PubMed: 17695343]
32. Hosic S; Puzan ML; Lake W; Zhou F; Koppes RA; Breault DT; Murthy SK; Koppes AN, Rapid prototyping of a multilayer microphysiological system for primary human intestinal epithelial culture. bioRxiv 2018, DOI: 10.1101/400721.

33. Ramadan Q; Ting FCW, In vitro micro-physiological immune-competent model of the human skin. Lab Chip 2016, 16 (10), 1899–1908. [PubMed: 27098052]
34. Stallcop LE; Alvarez-Garcia YR; Reyes-Ramos AM; Ramos-Cruz KP; Morgan MM; Shi YT; Li LJ; Beebe DJ; Domenech M; Warrick JW, Razor-printed sticker microdevices for cell-based applications. Lab Chip 2018, 18 (3), 451–462. [PubMed: 29318250]
35. Martinez AW; Phillips ST; Butte MJ; Whitesides GM, Patterned paper as a platform for inexpensive, low-volume, portable bioassays. Angew. Chem., Int. Ed 2007, 46 (8), 1318–1320.
36. de Gregorio R; Benet J; Katcho NA; Blas FJ; MacDowell LG, Semi-infinite boundary conditions for the simulation of interfaces: the Ar/CO2(s) model revisited. J. Chem. Phys 2012, 136 (10), 104703. [PubMed: 22423854]
37. Sato T; Vries RG; Snippert HJ; van de Wetering M; Barker N; Stange DE; van Es JH; Abo A; Kujala P; Peters PJ; Clevers H, Single Lgr5 stem cells build crypt-villus structures in vitro without a mesenchymal niche. Nature 2009, 459 (7244), 262–266. [PubMed: 19329995]
38. Lundholt BK; Scudder KM; Pagliaro L, A simple technique for reducing edge effect in cell-based assays. J. Biomol. Screen 2003, 8 (5), 566–570. [PubMed: 14567784]
39. Wang Y; Kim R; Hwang SJ; Dutton J; Sims CE; Allbritton NL, Analysis of Interleukin 8 Secretion by a Stem-Cell-Derived Human-Intestinal-Epithelial-Monolayer Platform. Anal. Chem 2018, 90 (19), 11523–11530. [PubMed: 30199234]
40. Goldberg RF; Austen WG; Zhang XB; Munene G; Mostafa G; Biswas S; McCormack M; Eberlin KR; Nguyen JT; Tatlidede HS; Warren HS; Narisawa S; Millan JL; Hodin RA, Intestinal alkaline phosphatase is a gut mucosal defense factor maintained by enteral nutrition. Proc. Natl. Acad. Sci. U. S. A 2008, 105 (9), 3551–3556. [PubMed: 18292227]
41. Kaiko GE; Ryu SH; Koues OI; Collins PL; Solnica-Krezel L; Pearce EJ; Pearce EL; Oltz EM; Stappenbeck TS, The Colonic Crypt Protects Stem Cells from Microbiota-Derived Metabolites. Cell 2016, 167 (4), 1137–1137. [PubMed: 27814510]
42. Miyoshi H; Stappenbeck TS, In vitro expansion and genetic modification of gastrointestinal stem cells in spheroid culture. Nat. Protoc 2013, 8 (12), 2471–2482. [PubMed: 24232249]
43. Umar S, Intestinal stem cells. Curr. Gastroenterol. Rep 2010, 12 (5), 340–348. [PubMed: 20683682]
44. Barker N, Adult intestinal stem cells: critical drivers of epithelial homeostasis and regeneration. Nat Rev Mol Cell Bio 2014, 15 (1), 19–33. [PubMed: 24326621]
45. Goodell MA; Nguyen H; Shroyer N, Somatic stem cell heterogeneity: diversity in the blood, skin and intestinal stem cell compartments. Nat Rev Mol Cell Bio 2015, 16 (5), 299–309. [PubMed: 25907613]
46. VanDussen KL; Carulli AJ; Keeley TM; Patel SR; Puthoff BJ; Magness ST; Tran IT; Maillard I; Siebel C; Kolterud A; Grosse AS; Gumucio DL; Ernst SA; Tsai YH; Dempsey PJ; Samuelson LC, Notch signaling modulates proliferation and differentiation of intestinal crypt base columnar stem cells. Development 2012, 139 (3), 488–497. [PubMed: 22190634]
47. Thorne CA; Chen IW; Sanman LE; Cobb MH; Wu LF; Altschuler SJ, Enteroid Monolayers Reveal an Autonomous WNT and BMP Circuit Controlling Intestinal Epithelial Growth and Organization. Dev. Cell 2018, 44 (5), 624–633 e4. [PubMed: 29503158]

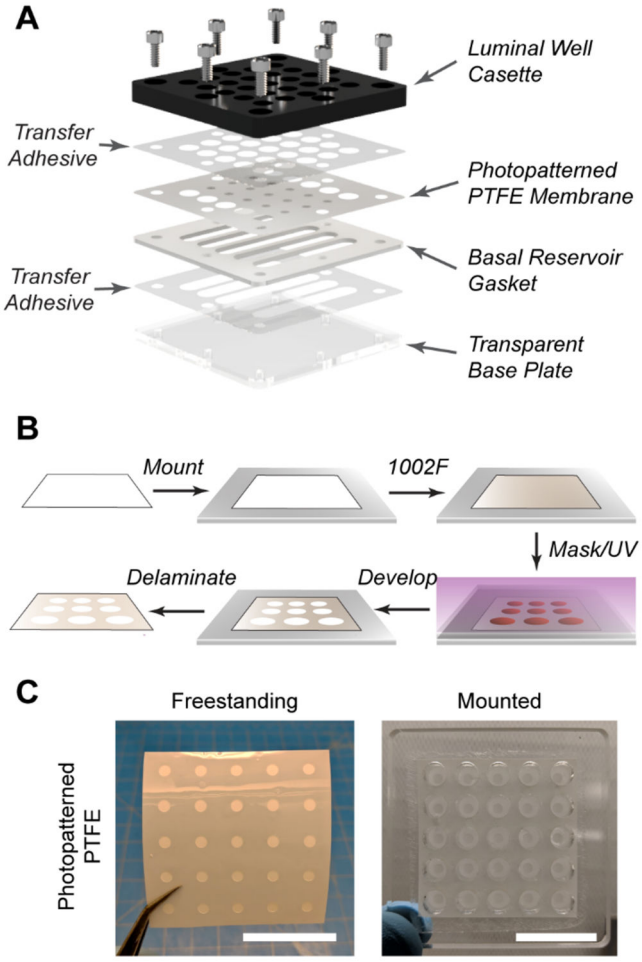

Figure 1.

Design of a scalable culture device with individually addressable z-axial gradients. (A) Rendering of device components and assembly configuration. (B) Photolithographic patterning of hydrophilic PTFE. (C) Photographs of patterned PTFE membranes, freestanding and mounted to a transparent cassette. Scale bars represent 30 mm.

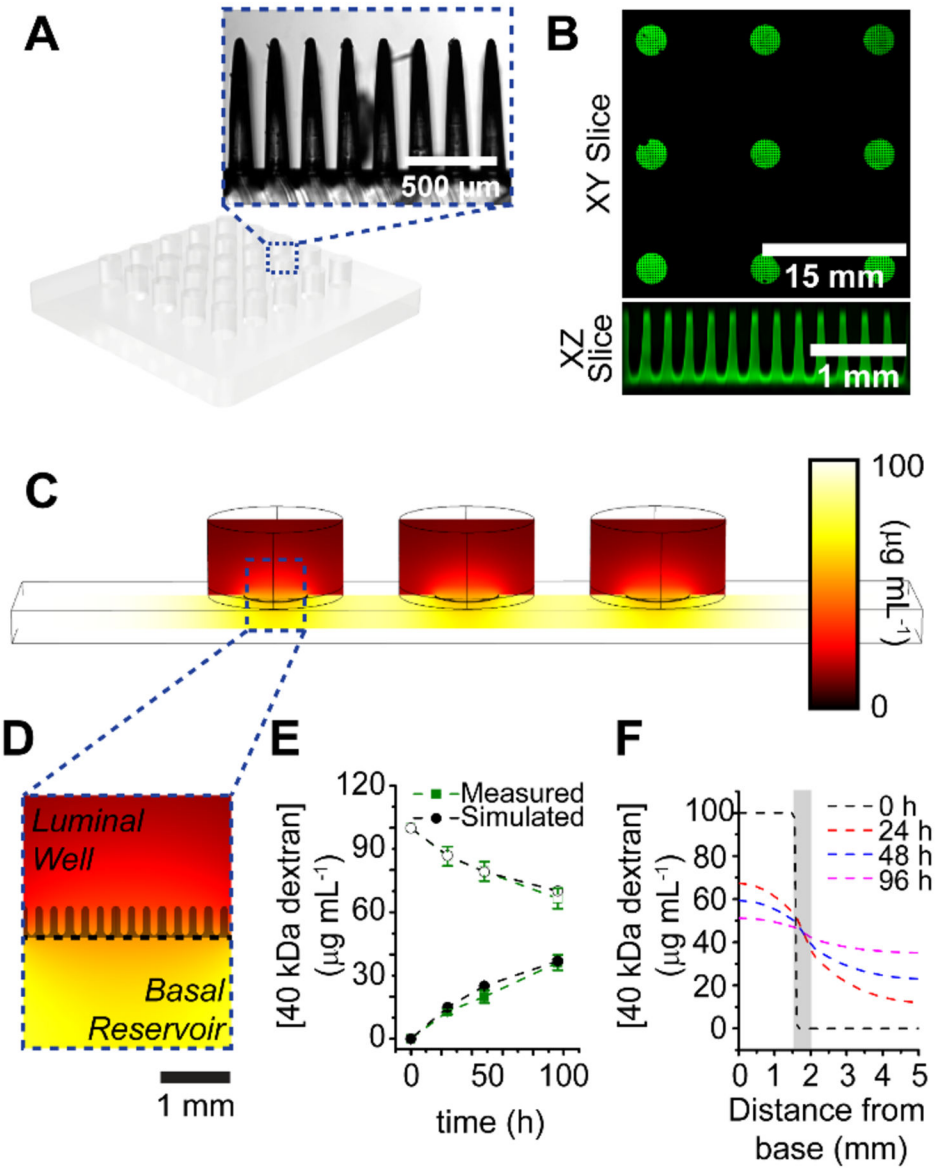

Figure 2.

Optimization of micromolding and diffusion window dimensions. (A) Schematic of PDMS stamp used for micromolding collagen, inset image depicts representative area of micropillars. (B) Stitched image of micromolded collagen scaffolds over patterned membranes, with slice view of scaffolds over a single diffusion window. (C) COMSOL modeling of 40 kDa fluorescein-dextran diffusion within a single lane of the device. Three luminal wells share a single basal reservoir, separated by a 7.07 mm^2 diffusion window. (D) Magnified image of single well, with collagen scaffold silhouetted to scale. (E) Experimental and simulated diffusion profiles of 40 kDa fluorescein-dextran over 96 h. Open shapes represent basal concentration, while closed shapes represent luminal concentration. (F) Simulated cut line profiles of dextran concentrations at different *z*-axial positions within a single well over time. The area shaded in grey represents the location and length of the crypts.

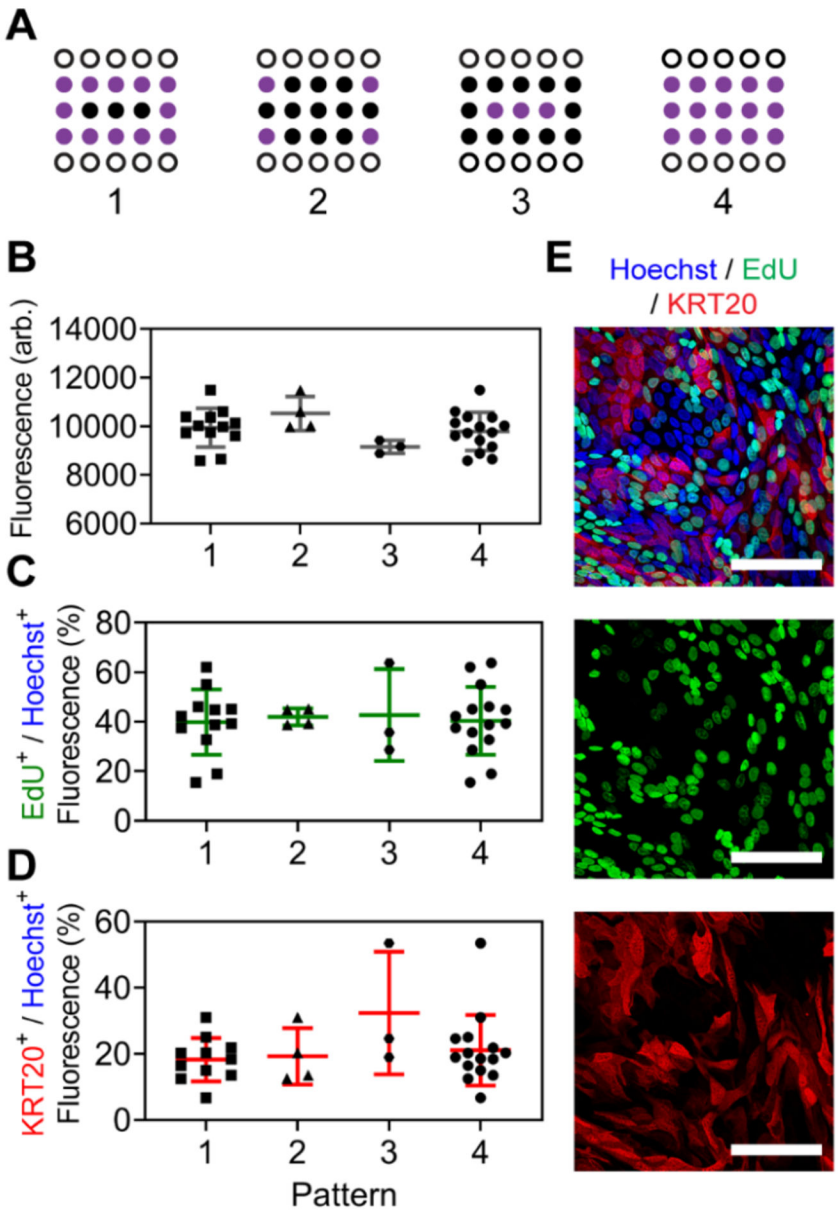

Figure 3.

Assessment of lateral edge effects when identical *z*-axial gradients are generated across the device. (A) Representative measurement patterns for studies. Open circles were used for basal reservoir access, while purple circles were averaged and compared. (B) Luminal measurements of fluorescein-dextran (40 kDa) after 24 h incubation at 37 °C. Basal reservoirs were filled with dye while luminal reservoirs were filled with buffer at t = 0. (C,D) Planar monolayer cultures of primary colonic epithelial cells were exposed to identical chemical gradients, and proliferative capacities (C) or differentiation status (D) were compared. (E) Representative images of cell monolayers assayed for DNA presence (Hoechst, blue), proliferation (EdU, green), and a general differentiation marker (KRT20, red). Scale bars represent 75 μm.

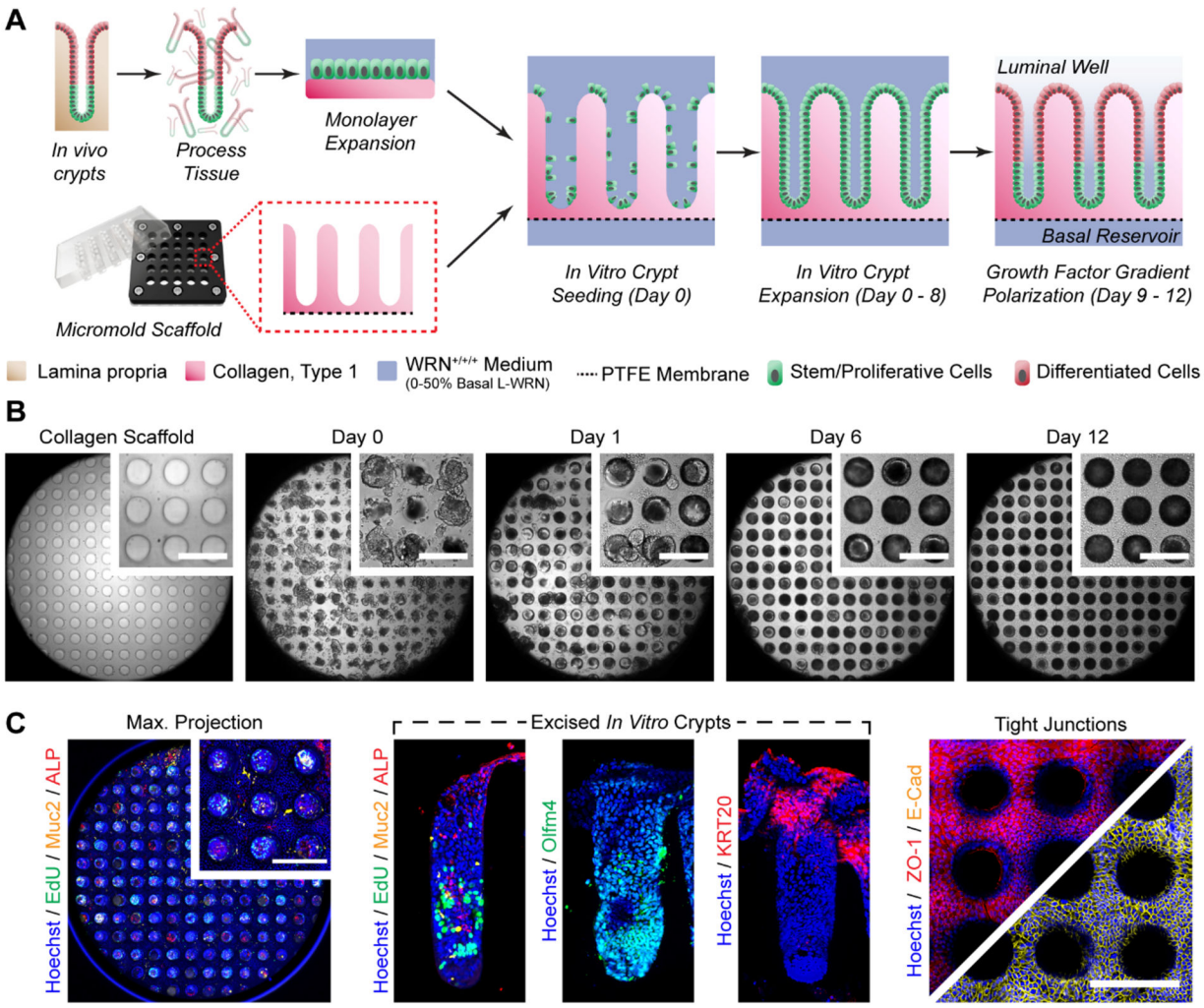

Figure 4.

Generation of *in vitro* colonic crypts. (A) Cell culture and device preparation for parallel *in vitro* crypt generation. (B) Bright field images of *in vitro* crypts during culture. Observable area encompasses the entire 3 mm dia. crypt area, while inset scale bars represent 250 μm. (C) Distributions of various biomarkers within *in vitro* crypts. A maximum projection was obtained from confocal imaging of the crypts along the *z*-axis and summing the images. Excised *in vitro* crypts were manually removed from the scaffolds and placed on their sides for imaging by standard fluorescence microscopy. The luminal cell plane was selected for confocal imaging of the tight junction markers. Inset scale bars represent 250 μm.

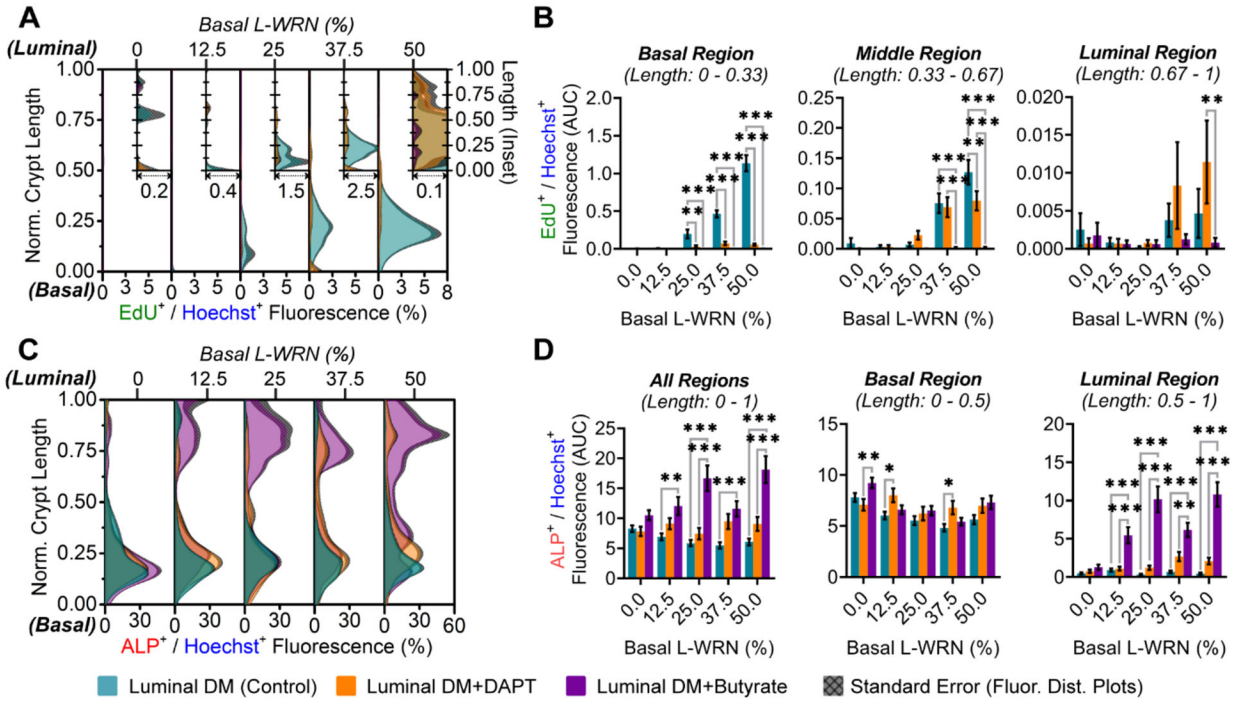

Figure 5.

Distributions of proliferative and differentiated cells within *in vitro* crypts. (A) Distribution of EdU^+ fluorescence normalized to Hoechst 33342^+ fluorescence (x-axis) along the crypt length (y-axis) under different chemical gradients. Cultures exposed to increasing basal concentrations of WRN across the array, and selected Notch regulators (DAPT and butyrate) through luminal differentiation media. The legend below panel C-D shows the color code for the different gradients that were formed, *i.e* .,for the curves depicted in the graphs. Inset plots are scaled for better visualization of distributions. (B) Total EdU^+ fluorescence within designated regions of the *in vitro* crypts. (C) Fluorescence distributions of ALP^+ fluorescence normalized to Hoechst 33342^+ fluorescence along the crypt axis. (D) Total ALP^+ fluorescence within designated regions of the *in vitro* crypts.